mathematics

MDPI

Article

Magnetic Impact on the Unsteady Separated Stagnation-Point Flow of Hybrid Nanofluid with Viscous Dissipation and Joule Heating

Nurul Amira Zainal [1,2], Roslinda Nazar [1,*], Kohilavani Naganthran [3,4] and Ioan Pop [5,6]

[1] Department of Mathematical Sciences, Faculty of Science and Technology, Universiti Kebangsaan Malaysia, Bangi 43600, Malaysia; nurulamira@utem.edu.my
[2] Fakulti Teknologi Kejuruteraan Mekanikal dan Pembuatan, Universiti Teknikal Malaysia Melaka, Hang Tuah Jaya, Durian Tunggal 76100, Malaysia
[3] Institute of Mathematical Sciences, Faculty of Science, Universiti Malaya, Kuala Lumpur 50603, Malaysia; kohi@um.edu.my
[4] Center for Data Analytics, Consultancy and Services, Faculty of Science, Universiti Malaya, Kuala Lumpur 50603, Malaysia
[5] Department of Mathematics, Babeş-Bolyai University, 400084 Cluj-Napoca, Romania; popm.ioan@yahoo.co.uk
[6] Academy of Romanian Scientists, 3 Ilfov Street, 050044 Bucharest, Romania
* Correspondence: rmn@ukm.edu.my

Abstract: The behaviour of magnetic impact on the unsteady separated stagnation-point flow of hybrid nanofluid with the influence of viscous dissipation and Joule heating is investigated numerically in this study. A new mathematical hybrid nanofluid model is developed, and similarity solutions are obtained in the form of ordinary differential equations (ODEs). The bvp4c approach in MATLAB is used to determine the reduced ODEs' estimated solutions. The influence of various physical parameters is scrutinised. The findings revealed that the skin friction coefficient increases with the increment of the nanoparticle volume fraction and the unsteadiness parameter. This observation is also applied to the heat transfer rate of the fluid. Additionally, the presence of the magnetic and acceleration parameter provides a significant result in the heat transfer performance. The addition of the Eckert number increased the temperature profile distribution, thereby spontaneously decreasing the heat transfer rate. The first solution is declared stable by the analysis of solution stability.

Keywords: MHD; unsteady flow; hybrid nanofluid; viscous dissipation; Joule heating

MSC: 34B15; 76D10; 76M55

Citation: Zainal, N.A.; Nazar, R.; Naganthran, K.; Pop, I. Magnetic Impact on the Unsteady Separated Stagnation-Point Flow of Hybrid Nanofluid with Viscous Dissipation and Joule Heating. *Mathematics* **2022**, *10*, 2356. https://doi.org/10.3390/math10132356

Received: 3 June 2022
Accepted: 28 June 2022
Published: 5 July 2022

1. Introduction

Hybrid nanofluids are the latest category of heat transfer fluids with great potential for industrial applications derived from the distribution of nanoparticles in conventional fluids. To create the appropriate combination of hybrid nanofluids, these fluids are made up of metallic or non-metallic particles. In a variety of applications, including heat transmission, hybrid nanofluids have been used in mechanical heat sinks, plate heat exchangers, and helical heat exchangers [1,2]. Previous research has shown that when nanoparticles are suspended in ordinary fluids, the heat transfer properties improve, increasing thermal conductivity [3]. However, selecting appropriate nanoparticles is one of the most important aspects of maintaining a stable hybrid nanofluid proportion. In relation to the aim of this study, some related references on nanofluids and hybrid nanofluids in various applications can be found in Rabiei et al. [4], Renuka et al. [5], Ur Rehman et al. [6], and Connolly et al. [7]. We also mention some recently published papers by Kamis et al. [8], Nadeem et al. [9], Elsaid et al. [10], Hassan et al. [11], and Sheikholeslami [12], who presented a

numerical simulation of boundary layer flow in a hybrid nanofluid considering various physical phenomena.

The inclusion of magnetohydrodynamics (MHD) has piqued the interest of scholars due to its importance in numerous fields, including geology, astrophysics, drug industries, cosmology, MHD generators, and seismology. According to Khalili et al. [13], the role of MHD is to restrict fluid flow by aligning it to magnetic fields. Devi and Devi [14] studied the impacts of MHD boundary layer flow in a hybrid nanofluid over a stretching sheet with a suction effect. They discovered that the hybrid nanofluid has a higher heat transfer rate than nanofluid in a magnetic environment. Meanwhile, Zainal et al. [15] noticed that the occurrence of a suction parameter and MHD tends to slow fluid motion due to the synchronism of the magnetic and electric fields caused by the Lorentz force formation. Recently, Khashi'ie et al. [16] investigated the unsteady squeezing flow in a horizontal channel with the influence of a magnetic field in a hybrid nanofluid. Up to now, many scientific researchers have investigated the effect of magnetic field parameters in Newtonian or non-Newtonian fluid flows over stretching/shrinking surfaces by considering various impacts, for example, Yashkun et al. [17], Zainal et al. [18], Aly et al. [19], Shafee et al. [20], and Dinarvand [21].

The Joule heating mechanism demonstrates an evolving appeal in massive engineering and manufacturing processes, including the electrical and electronic device configurations. The main benefit of Joule heating is that it transports electrical strength to reduce damage by lowering the current. According to Reddy and Reddy [22], the nanofluid temperature in the boundary layer flow is raised using this control parameter. Sheikholeslami and Ganji [23] investigated the nanofluid behaviour with the appearance of magnetic effect and Joule heating. A comparison study has been conducted by Khashi'ie et al. [24,25] in hybrid nanofluid and heat transfers towards a permeable shrinking surface by including the Joule heating. Naseem et al. [26] discovered that the temperature profile increases as the Eckert number rises. Many other researchers have contributed to the study of fluid flow and heat transfer by taking Joule heating phenomena into account, and thus, more detail can be found in the references mentioned therein, as seen in Daniel et al. [27], Khan et al. [28], Yan et al. [29], and Mahanthesh et al. [30].

Nevertheless, the study mentioned above is about constant flows. In some cases, a change in the free stream velocity or the surface temperature might cause the flow to become unstable. Hayat et al. [31] observed the unsteady three-dimensional flow over an exponential surface, considering viscous dissipation effects and Joule heating using boundary layer approximations. In another investigation, Chaudhary and Choudhary [32] discovered that as the unsteadiness parameter improves, the thermal boundary layer thickness and the heat transfer rate decline. Meanwhile, according to Ahmed et al. [33], higher amounts of the unsteadiness parameter improve the distribution of temperature, while increasing the Eckert number substantially improves the temperature distribution in the Maxwell fluid. Mahanthesh et al. [30] concluded that the viscous dissipation and thermal radiation influences are critical in the cooling and heating processes; hence, they should be preserved to a reasonable level in cooling systems. As for references, Malekian et al. [34], Zainal et al. [35,36], Rehman and Salleh [37], and Waini et al. [38] have scrutinised various analytical and numerical investigations to explore the unsteady-state behaviour in nanofluid and hybrid nanofluid flow.

A previous study by Dholey [39] only considers the viscous flow without observing the heat transfer in his mathematical model. Today, experimental and numerical research have shown that nanofluid reacts as a better heat transfer fluid when compared to viscous fluid. Motivated by the outstanding work of Dholey [39], the main objective of this study is to broaden his research by employing hybrid nanofluid flow in a magnetic environment of the boundary layer and heat transfer. Hence, a new mathematical hybrid nanofluid model is introduced. The current study also aims to fill a research gap in the existing literature, particularly in studying the unsteady separated stagnation-point flow by including viscous dissipation and the Joule heating impact. In this particular instance, another objective

of this study is to explore the effect of designated physical parameters in the context of hydrodynamic flow and heat transfer of a hybrid nanofluid. Thus, to solve the stated problem, the bvp4c scheme in the MATLAB package is used. Comparative results for a specific case have been obtained, revealing a strong correlation between previous work and the existing outcomes. Since the appearance of dual solutions is observed, the third objective of this study is to perform a stability analysis to evaluate the solution's dependability. Overall, we believe that an extensive study on the unsteady separated stagnation flows combined with the application of mathematical knowledge should be intensified to gain a better understanding due to its major significance in many industrial applications such as start-up processes and periodic fluid motion. This will lead to progressive improvements in the efficiency, durability, and cost of many fluid dynamic devices in order to establish new and advanced heat transfer technology.

2. Mathematical Formulations

Let us consider the unsteady MHD separated stagnation-point in two-dimensional flow of a hybrid nanofluid, as shown in Figure 1, where (x, y) are Cartesian coordinates with the x-axis measured along the shrinking surface, y is in the direction normal to the surface, and the flow is at $y \geq 0$. It is assumed that the velocity of the shrinking surface is $u_w(t) = u_0(t)$ and that of the far-field (inviscid hybrid nanofluid flow) is $u_e(x,t) = a\frac{x-x_0(t)}{t_{ref}-\beta t} + u_0(t)$, where t denotes time. Next, the magnetic field $B(t_1)$ is $B(t_1) = B_0/\sqrt{(t_0 - \beta t_1)}$, where B_0 is the applied magnetic field strength, β is a parameter showing the unsteadiness of the problem, and $t_0 = \left(\nu_f t_{ref}/l^2\right)$ and $t_1 = \left(\nu_f t/l^2\right)$ are the dimensionless forms of the constant reference value of time t_{ref} and general time t. From the definition of $B(t_1)$, it can be concluded that $(t_0 - Bt_1) > 0$, which gives $t_1 < t_0/\beta$. The surface temperature $T_w(x,t)$ of the sheet is $T_w(x,t) = T_\infty + T_0(x/l)^2/(1-\beta t)^2$, where $T_0(> 0)$ is the sheet characteristic temperature, l is the sheet length characteristic, and T_∞ represents the free stream temperature. The working fluid contains two types of nanoparticles, namely, alumina (Al_2O_3) and copper (Cu), hence forming a hybrid nanofluid (Al_2O_3-Cu/H_2O) with water (H_2O) as the base fluid. In this study, we also consider the effects of viscous dissipation and Joule heating, which are included in the energy equation below.

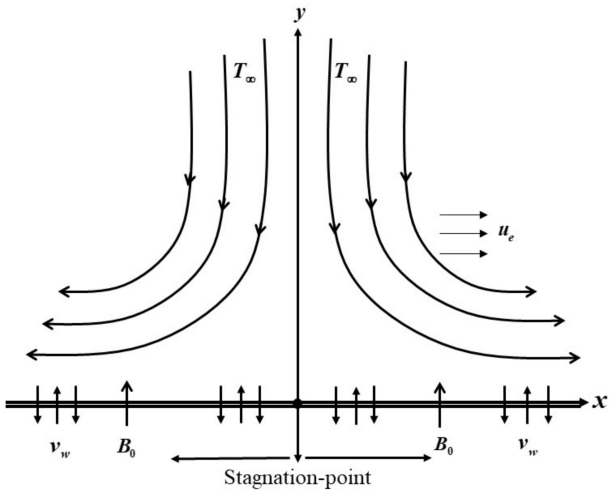

Figure 1. Illustration of the problem configuration.

Based on the above proposed assumptions, the following set of governing equations can be expressed in Cartesian coordinates (x, y), as follows (see Dholey [39]; Devi and Devi [14]):

$$\frac{\partial u}{\partial x} + \frac{\partial v}{\partial y} = 0, \tag{1}$$

$$\frac{\partial u}{\partial t} + u\frac{\partial u}{\partial x} + v\frac{\partial u}{\partial y} = \frac{\partial u_e}{\partial t} + u_e\frac{du_e}{dx} + \frac{\mu_{hnf}}{\rho_{hnf}}\left(\frac{\partial^2 u}{\partial y^2}\right) - \frac{\sigma_{hnf}}{\rho_{hnf}}B^2(u-u_e), \tag{2}$$

$$\frac{\partial T}{\partial t} + u\frac{\partial T}{\partial x} + v\frac{\partial T}{\partial y} = \frac{k_{hnf}}{(\rho C_p)_{hnf}}\left(\frac{\partial^2 T}{\partial y^2}\right) + \frac{\mu_{hnf}}{(\rho C_p)_{hnf}}\left(\frac{\partial u}{\partial y}\right)^2 + \frac{\sigma_{hnf}}{(\rho C_p)_{hnf}}B^2(u-u_e)^2, \tag{3}$$

along with the boundary conditions

$$\begin{aligned} &u = \lambda u_w(x,t),\ v = 0,\ T = T_w(x,t)\ \text{ at }\ y = 0,\\ &u \to u_e(x,t),\ T \to T_\infty\ \text{ as } y \to \infty. \end{aligned} \tag{4}$$

From the above condition, $\lambda = 0$ is for a static sheet; $\lambda < 0$ and $\lambda > 0$ denote the shrinking/stretching parameter, respectively; T is the temperature of the hybrid nanofluid; T_0 is the characteristic temperature of the hybrid nanofluid; and l is the length characteristic of the sheet. In addition, μ_{hnf} is the dynamic viscosity; k_{hnf} is the heat/thermal conductivity; and ρ_{hnf} and $(\rho C_p)_{hnf}$ are the density and heat capacity, respectively. Following that, Tables 1 and 2 demonstrate the hybrid nanofluid correlations and the nanoparticle's characteristics, respectively, where ϕ_1 is Al_2O_3 (alumina) nanoparticle and ϕ_2 is Cu (copper) nanoparticle. Referring to the experimental work, the characteristic temperature of the hybrid nanofluid T_0 in the solution process is in the range of 25°C–50°C [3,40].

Table 1. Correlations of hybrid nanofluid (see Takabi and Salehi [40]).

Characteristics	Alumina-Copper/Water (Al_2O_3–Cu/H_2O)
Dynamic viscosity, μ_{hnf}	$\mu_{hnf}/\mu_f = \left(1-\phi_{hnf}\right)^{-2.5}$
Heat capacity, $(\rho C_p)_{hnf}$	$(\rho C_p)_{hnf} - \left(1-\phi_{hnf}\right)(\rho C_p)_f = \phi_1(\rho C_p)_{Al_2O_3} + \phi_2(\rho C_p)_{Cu}$
Density, ρ_{hnf}	$\rho_{hnf} = \left(1-\phi_{hnf}\right)\rho_f + \phi_1\rho_{Al_2O_3} + \phi_2\rho_{Cu}$
Thermal conductivity, k_{hnf}	$\frac{k_{hnf}}{k_f} = \left[\frac{\left(\frac{\phi_1 k_{Al_2O_3}+\phi_2 k_{Cu}}{\phi_{hnf}}\right)+2k_f+2\left(\phi_1 k_{Al_2O_3}+\phi_2 k_{Cu}\right)-2\phi_{hnf}k_f}{\left(\frac{\phi_1 k_{Al_2O_3}+\phi_2 k_{Cu}}{\phi_{hnf}}\right)+2k_f-\left(\phi_1 k_{Al_2O_3}+\phi_2 k_{Cu}\right)+\phi_{hnf}k_f}\right]$
Electrical conductivity, σ_{hnf}	$\frac{\sigma_{hnf}}{\sigma_f} = \left[\frac{\left(\frac{\phi_1 \sigma_{Al_2O_3}+\phi_2 \sigma_{Cu}}{\phi_{hnf}}\right)+2\sigma_f+2\left(\phi_1 \sigma_{Al_2O_3}+\phi_2 \sigma_{Cu}\right)-2\phi_{hnf}\sigma_f}{\left(\frac{\phi_1 \sigma_{Al_2O_3}+\phi_2 \sigma_{Cu}}{\phi_{hnf}}\right)+2\sigma_f-\left(\phi_1 \sigma_{Al_2O_3}+\phi_2 \sigma_{Cu}\right)+\phi_{hnf}\sigma_f}\right]$

Table 2. Base fluid and nanoparticle properties (see Oztop and Abu-Nada [41]).

Properties	ρ (kg/m^3)	k (W/mK)	C_p (J/kgK)
Cu	8933	400	385
H_2O	997.1	0.613	4179
Al_2O_3	3970	40	765

We now introduce the appropriate similarity variables pursuing Dholey [39], as follows:

$$\begin{aligned} &u = \alpha\frac{x-x_0(t)}{t_{ref}-\beta t}f'(\eta) + u_0(t),\ v = -\alpha\sqrt{\frac{\nu_f}{t_{ref}-\beta t}}f(\eta),\\ &\theta(\eta) = \frac{T-T_\infty}{T_w(x,t)-T_\infty},\ \eta = \frac{y}{\left[\nu_f\left(t_{ref}-\beta t\right)\right]^{1/2}}, \end{aligned} \tag{5}$$

where $\alpha(>0)$ is a constant, known as the acceleration parameter; $x_0(t)$ denotes displacement of the sheet, so that $u_0(t) = \partial x_0(t)/\partial t$; and the prime denote differentiation with respect to η.

Substituting (5) into Equations (2) and (3), we obtain the following ordinary (similarity) differential equations and boundary conditions:

$$\frac{\mu_{hnf}/\mu_f}{\rho_{hnf}/\rho_f} f''' + \alpha f f'' + \alpha\left(1 - f'^2\right) - \beta\left(f' + \frac{\eta}{2} f'' - 1\right) - \frac{\sigma_{hnf}/\sigma_f}{\rho_{hnf}/\rho_f} M(f' - 1) = 0, \tag{6}$$

$$\begin{aligned} &\frac{1}{\Pr}\frac{k_{hnf}/k_f}{(\rho C_p)_{hnf}/(\rho C_p)_f}\theta'' + f\theta' - 2f'\theta - \beta\left(2\theta + \frac{\eta}{3}\theta'\right) \\ &+ \frac{Ec}{(\rho C_p)_{hnf}/(\rho C_p)_f}\left[f''^2 + \frac{\sigma_{hnf}}{\sigma_f} M(1 - f')\right] = 0, \end{aligned} \tag{7}$$

$$\begin{aligned} f(0) = 0,\ f'(0) = \lambda,\ \theta(0) = 1, \\ f'(\eta) \to 1,\ \theta(\eta) \to 0,\ \text{as}\ \eta \to \infty. \end{aligned} \tag{8}$$

Here, Pr is the Prandtl number, M is the magnetic field parameter, and Ec is the Eckert number, which are given by

$$\Pr = \frac{(\rho C_p)_f}{k_f},\ M = \frac{\sigma_f B_0^2}{\alpha \rho_f},\ Ec = \frac{u_w^2}{C_p(T_w - T_\infty)}. \tag{9}$$

As for the quantities of physical interest, now, we have

$$\tau_w = \mu_{hnf}\left(\frac{\partial v}{\partial x} + \frac{\partial u}{\partial y}\right)_{y=0}, q_w = -k_{hnf}\left(\frac{\partial T}{\partial x} + \frac{\partial T}{\partial y}\right)_{y=0}, \tag{10}$$

where τ_w and q_w present the shear stress and the heat flux at a point on the surface of the sheet, respectively. By employing (5) and (10), we have

$$\tau_w = \alpha \frac{\left(\mu_{hnf}/\mu_f\right)[x - x_0(t)]}{\left[\nu_f\left(t_{ref} - \beta t\right)\right]^{3/2}} f''(0), q_w = \alpha \frac{\left(k_{hnf}/k_f\right)[x - x_0(t)]}{\left[\nu_f\left(t_{ref} - \beta t\right)\right]^{1/2}}\left[-\theta'(0)\right]. \tag{11}$$

Here, $f''(0)$ and $-\theta'(0)$ measure the coefficient of skin friction and heat transfer from the sheet's surface, respectively.

3. Analysis of Solution Stability

We test the fact that the dual solutions of the boundary value problem (6)–(8) are stable or unstable by performing a stability analysis. In this respect, we follow Merkin [42], who showed that the first solutions are stable or realisable, while the second solutions are unstable or physically unreliable. As in Weidman et al. [43], we introduce the new dimensionless time variable $\Gamma = \alpha t/\left(t_{ref} - \beta t\right)$. The use of Γ is associated with an initial value problem and is consistent with the question of which solution is reliable in practice. As there have been various solutions to the boundary value problem (6) and (7), an investigation of solution stability is conducted. Following that, new similarity solutions are now described in a subsequent manner

$$\begin{aligned} &u = \alpha\frac{x - x_0}{t_{ref} - \beta t}\frac{\partial f}{\partial \eta}(\eta, \Gamma) + u_0, v = -\alpha\sqrt{\frac{\nu_f}{t_{ref} - \beta t}} f(\eta, \Gamma), \\ &\theta(\eta, \Gamma) = \frac{T - T_\infty}{T_w - T_\infty},\ \eta = \frac{y}{\left[\nu_f\left(t_{ref} - \beta t\right)\right]^{1/2}}, \Gamma = \frac{\alpha}{t_{ref} - \beta t} t. \end{aligned} \tag{12}$$

Equations (6) and (7), as well as boundary conditions (8), are turned into the following equations by employing (12), resulting in

$$\begin{aligned} &\frac{\mu_{hnf}/\mu_f}{\rho_{hnf}/\rho_f}\frac{\partial^3 f}{\partial \eta^3} + \alpha f\frac{\partial^2 f}{\partial \eta^2} + \alpha\left[1 - \left(\frac{\partial f}{\partial \eta}\right)^2\right] - \beta\left(\frac{\partial f}{\partial \eta} + \frac{\eta}{2}\frac{\partial^2 f}{\partial \eta^2} - 1\right) \\ &- \frac{\sigma_{hnf}/\sigma_f}{\rho_{hnf}/\rho_f} M\left(\frac{\partial f}{\partial \eta} - 1\right) - (1 + \beta\Gamma)\frac{\partial^2 f}{\partial \eta \partial \Gamma} = 0, \end{aligned} \tag{13}$$

$$\begin{aligned}&\frac{1}{\mathrm{Pr}}\frac{k_{hnf}/k_f}{(\rho C_p)_{hnf}/(\rho C_p)_f}\frac{\partial^2\theta}{\partial\eta^2}+f\frac{\partial\theta}{\partial\eta}-2\frac{\partial f}{\partial\eta}\theta-\beta\left(2\theta+\frac{\eta}{3}\frac{\partial\theta}{\partial\eta}\right)\\&+\frac{Ec}{(\rho C_p)_{hnf}/(\rho C_p)_f}\left[\left(\frac{\partial^2\theta}{\partial\eta^2}\right)^2+\frac{\sigma_{hnf}}{\sigma_f}M\left(1-\frac{\partial f}{\partial\eta}\right)\right]-(1+\beta\Gamma)\frac{\partial\theta}{\partial\Gamma}=0,\end{aligned}\tag{14}$$

$$\begin{aligned}&f(0,\Gamma)=0,\ \frac{\partial f}{\partial\eta}(0,\Gamma)=\lambda,\ \theta(0,\Gamma)=1,\\&\frac{\partial f}{\partial\eta}(\eta,\Gamma)\to 1,\ \theta(\eta,\Gamma)\to 0\text{ as }\eta\to\infty.\end{aligned}\tag{15}$$

Then, consider the perturbation function as follows (refer to Weidman et al. [43]):

$$\begin{aligned}f(\eta,\Gamma)&=f_0(\eta)+e^{-\omega\Gamma}F(\eta),\\\theta(\eta,\Gamma)&=\theta_0(\eta)+e^{-\omega\Gamma}I(\eta),\end{aligned}\tag{16}$$

where $F(\eta)$ and $I(\eta)$ are relatively small to $f_0(\eta)$ and $\theta_0(\eta)$, while ω signifies the eigenvalue. Substituting Equation (16) into Equations (13) and (14), we have

$$\begin{aligned}&\frac{\mu_{hnf}/\mu_f}{\rho_{hnf}/\rho_f}\frac{\partial^3F}{\partial\eta^3}+\alpha\left(f_0\frac{\partial^2F}{\partial\eta^2}+2\frac{\partial f_0}{\partial\eta}\frac{\partial F}{\partial\eta}+\frac{\partial^2f_0}{\partial\eta^2}F\right)\\&-\beta\left(\frac{\eta}{2}\frac{\partial^2F}{\partial\eta^2}+\frac{\partial F}{\partial\eta}\right)-\left(\frac{\sigma_{hnf}/\sigma_f}{\rho_{hnf}/\rho_f}M-\omega\right)\frac{\partial F}{\partial\eta}=0,\end{aligned}\tag{17}$$

$$\begin{aligned}&\frac{1}{\mathrm{Pr}}\left(\frac{k_{hnf}/k_f}{(\rho C_p)_{hnf}/(\rho C_p)_f}\right)\frac{\partial^2I}{\partial\eta^2}+f_0\frac{\partial I}{\partial\eta}+F\frac{\partial\theta_0}{\partial\eta}-2\left(I\frac{\partial f_0}{\partial\eta}+\theta_0\frac{\partial F}{\partial\eta}\right)-\beta\left(2I+\frac{\eta}{2}\frac{\partial I}{\partial\eta}\right)\\&+\frac{Ec}{(\rho C_p)_{hnf}/(\rho C_p)_f}\left[2\frac{\partial^2f_0}{\partial\eta^2}\frac{\partial^2F}{\partial\eta^2}-\frac{\sigma_{hnf}}{\sigma_f}2M\left(\frac{\partial f_0}{\partial\eta}-\frac{\partial F}{\partial\eta}+\frac{\partial f_0}{\partial\eta}\frac{\partial F}{\partial\eta}\right)\right]+\omega I=0,\end{aligned}\tag{18}$$

$$F(0)=0,\ \frac{\partial F}{\partial\eta}(0)=0,\ I(0)=0,\ \frac{\partial F}{\partial\eta}(\eta)\to 0,\ I(\eta)\to 0.\tag{19}$$

Eventually, by setting $\Gamma\to 0$ and by implementing the linearisation process, the solution to the linearised eigenvalue problem is identified as follows:

$$\frac{\mu_{hnf}/\mu_f}{\rho_{hnf}/\rho_f}F'''+\alpha\left(f_0F''+2f_0{}'F'+f_0{}''F\right)-\beta\left(\frac{\eta}{2}F''+F'\right)-\left(\frac{\sigma_{hnf}/\sigma_f}{\rho_{hnf}/\rho_f}M-\omega\right)F'=0,\tag{20}$$

$$\begin{aligned}&\frac{1}{\mathrm{Pr}}\left(\frac{k_{hnf}/k_f}{(\rho C_p)_{hnf}/(\rho C_p)_f}\right)I''+f_0I'+F\theta_0{}'-2(If_0{}'+\theta_0F')-\beta(2I+\tfrac{\eta}{2}I')\\&+\frac{Ec}{(\rho C_p)_{hnf}/(\rho C_p)_f}\left[2f''{}_0F''-\frac{\sigma_{hnf}}{\sigma_f}2M(f_0{}'-F'+f_0{}'F')\right]+\omega I=0,\end{aligned}\tag{21}$$

$$\begin{aligned}&F(0)=0,\ F'(0)=0,I(0)=0,\\&F'(\eta)\to 0,\ I(\eta)\to 0.\end{aligned}\tag{22}$$

To this extent, $F''(0)=1$ replaces $F'(\eta)\to 0$ as $\eta\to\infty$ in boundary conditions (22) (see Harris et al. [44]). Following that, the analysis of the finding is comprehensively described in the following section.

4. Analysis of Findings

This section discusses the effect of various physical parameters, where the results are shown graphically in Figures 2–13. The conclusions are drawn for the flow field and other physical quantities of interest. The bvp4c solver in MATLAB software was used to solve Equations (6) and (7) with respect to boundary conditions (8), numerically. The reliability of the current results is confirmed by comparing the numerical data with Lok and Pop [45], Ishak et al. [46], and Wang [47], as reported in Table 3. Since the present outcomes are consistent, we believe the obtained results are valid and trustworthy. This also proves that the recommended mathematical model for this problem is appropriate. The influence of specific physical characteristics is then investigated, and the results are presented in graphical form.

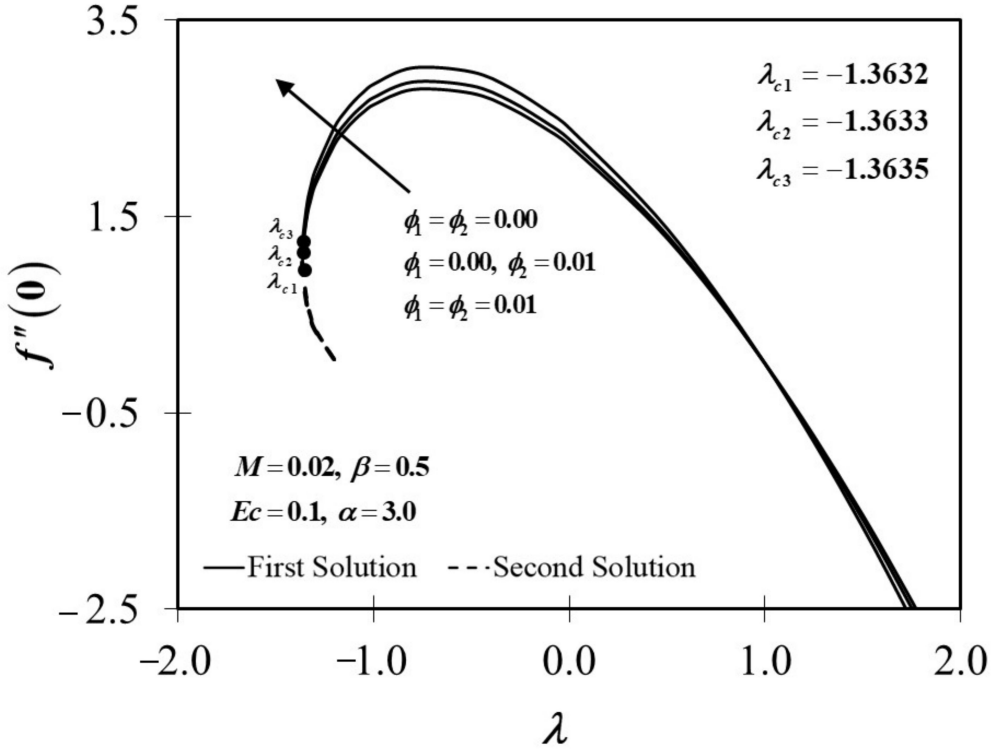

Figure 2. $f''(0)$ versus λ with specific ϕ.

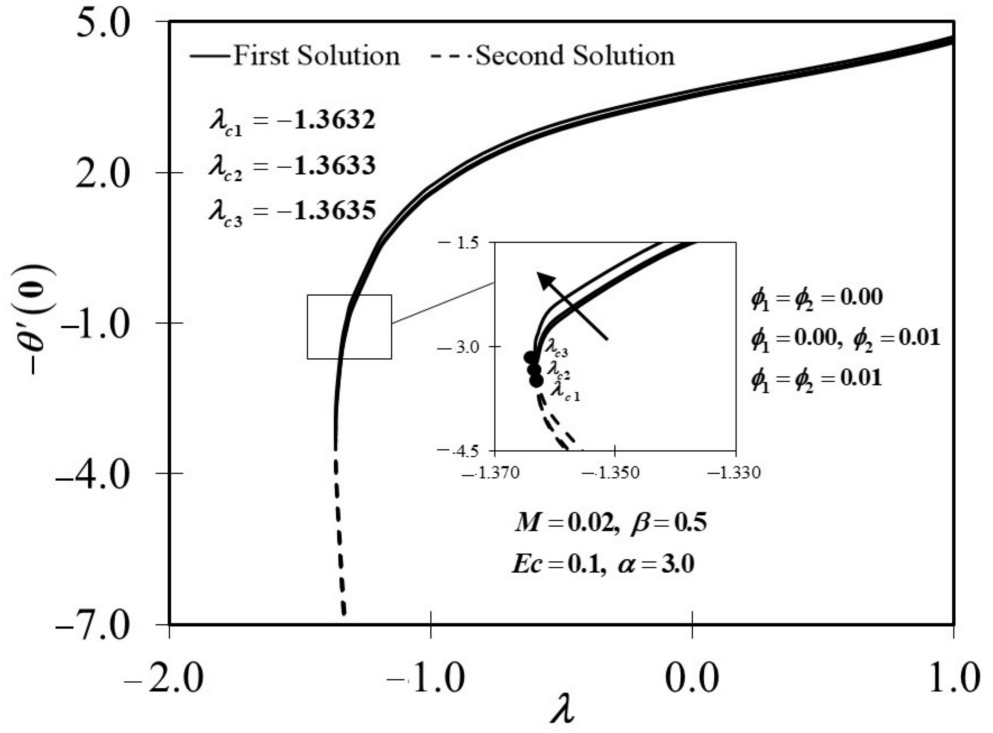

Figure 3. $-\theta'(0)$ versus λ with specific ϕ.

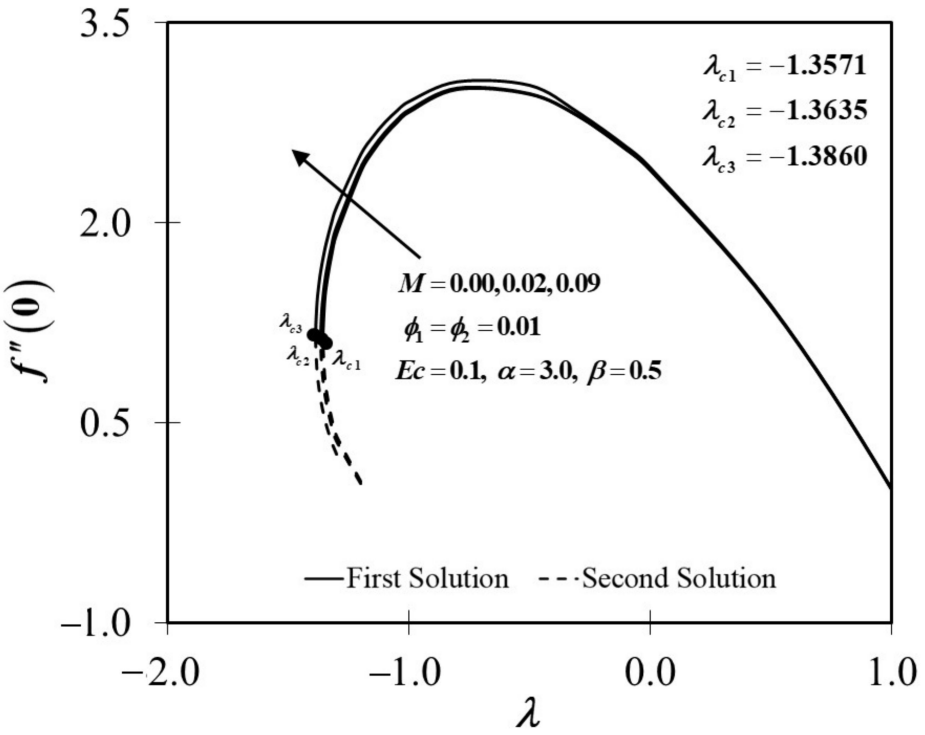

Figure 4. $f''(0)$ versus λ with specific M.

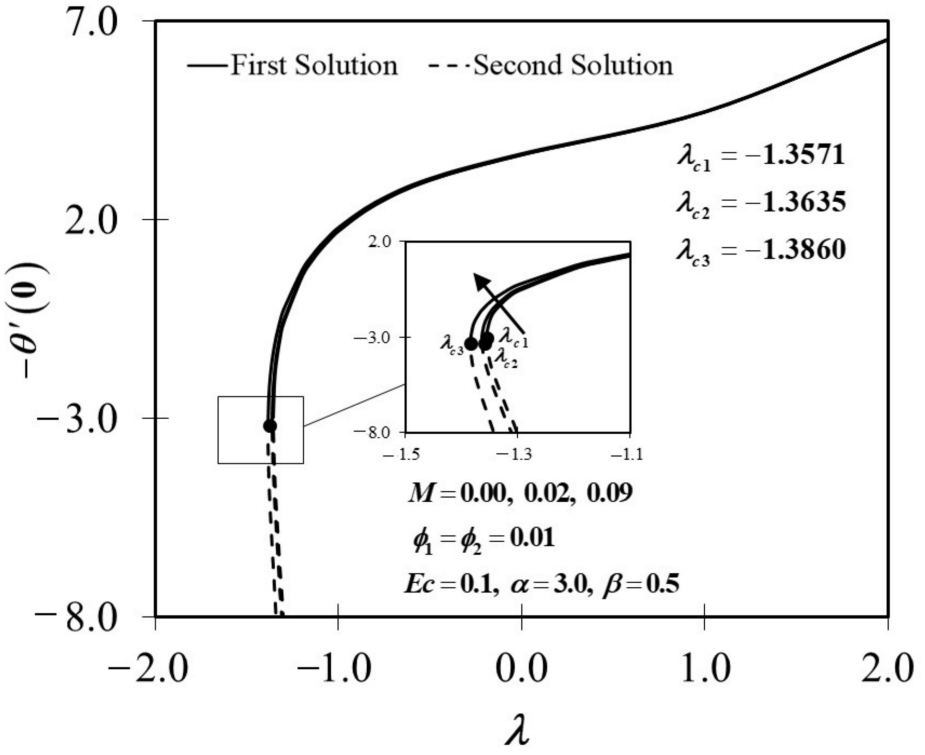

Figure 5. $-\theta'(0)$ versus λ with specific M.

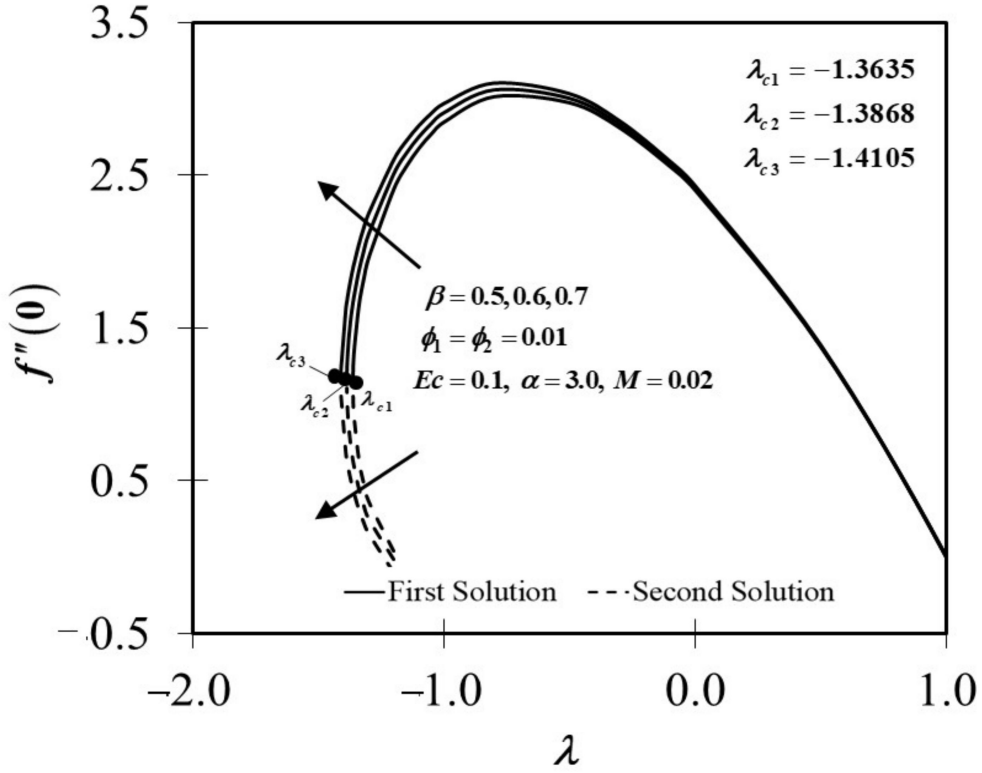

Figure 6. $f''(0)$ versus λ with specific β.

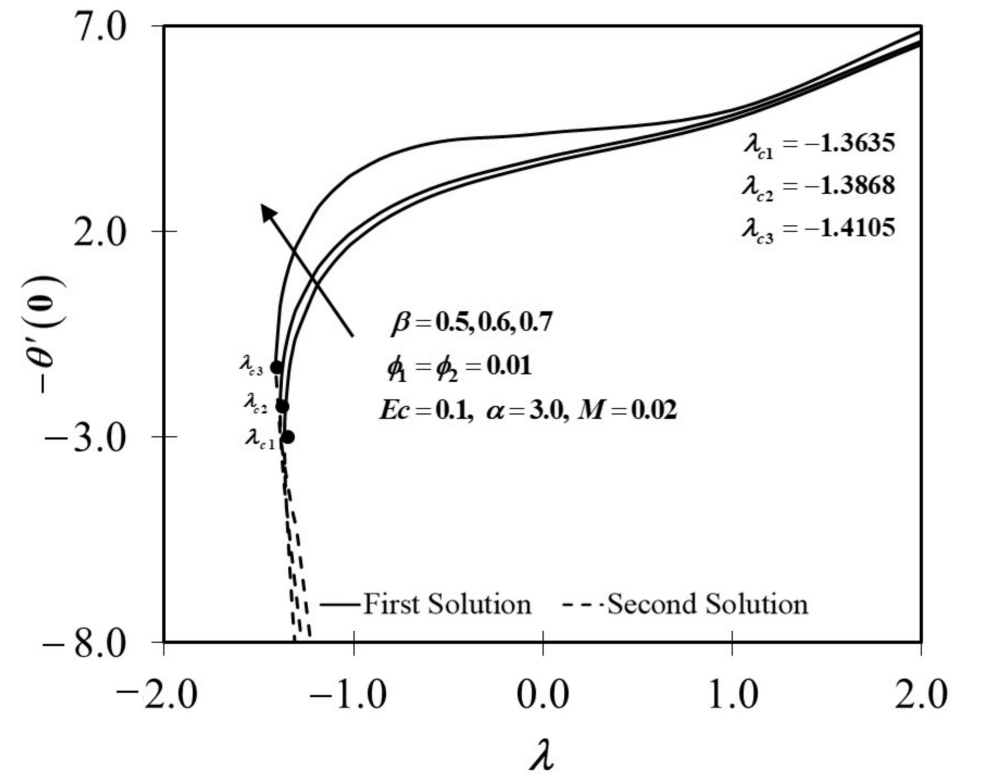

Figure 7. $-\theta'(0)$ versus λ with specific β.

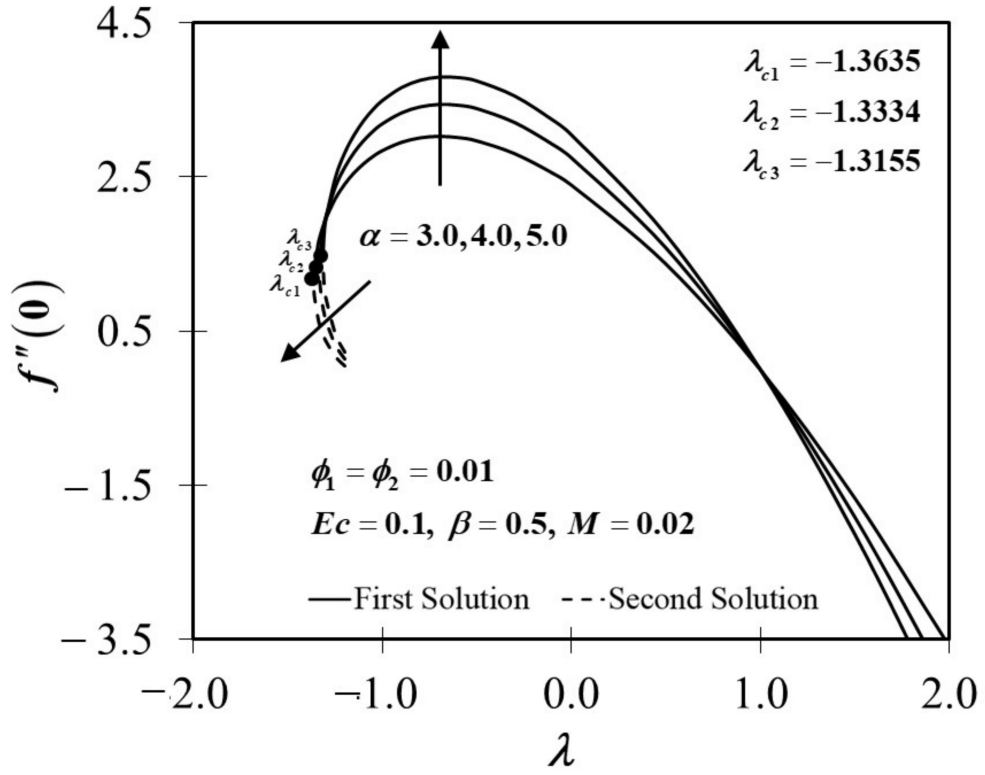

Figure 8. $f''(0)$ versus λ with specific α.

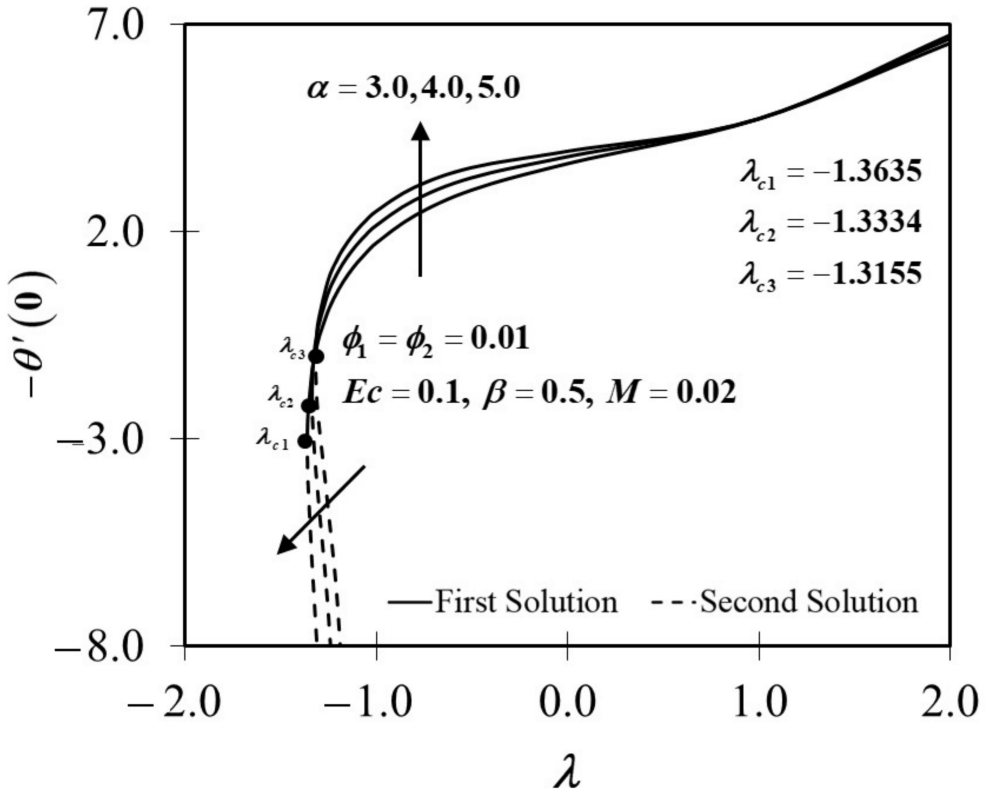

Figure 9. $-\theta'(0)$ versus λ with specific α.

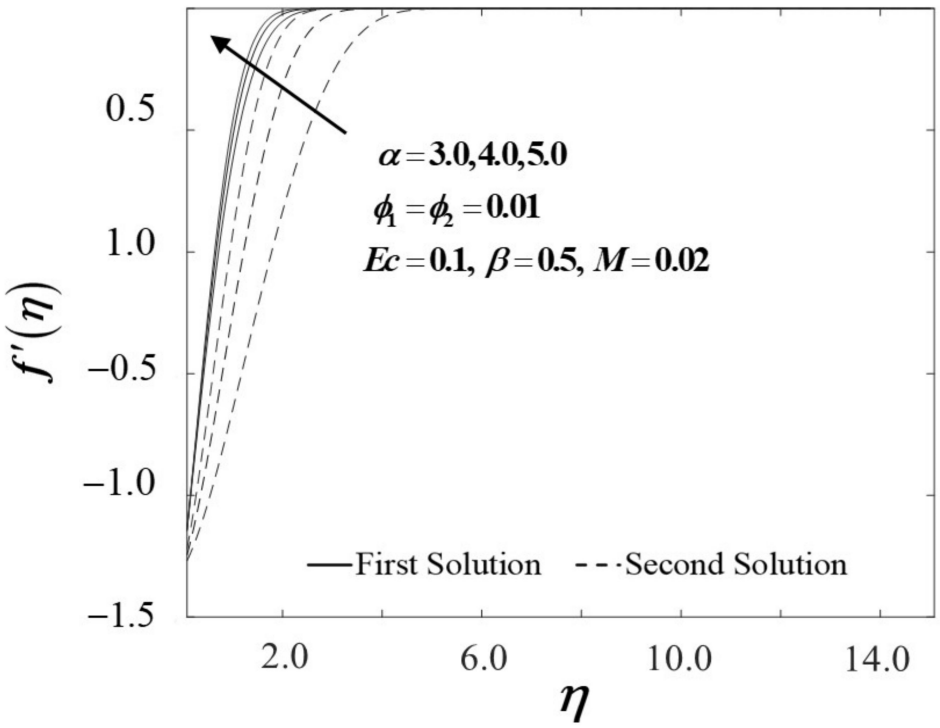

Figure 10. $f'(\eta)$ versus η with specific α.

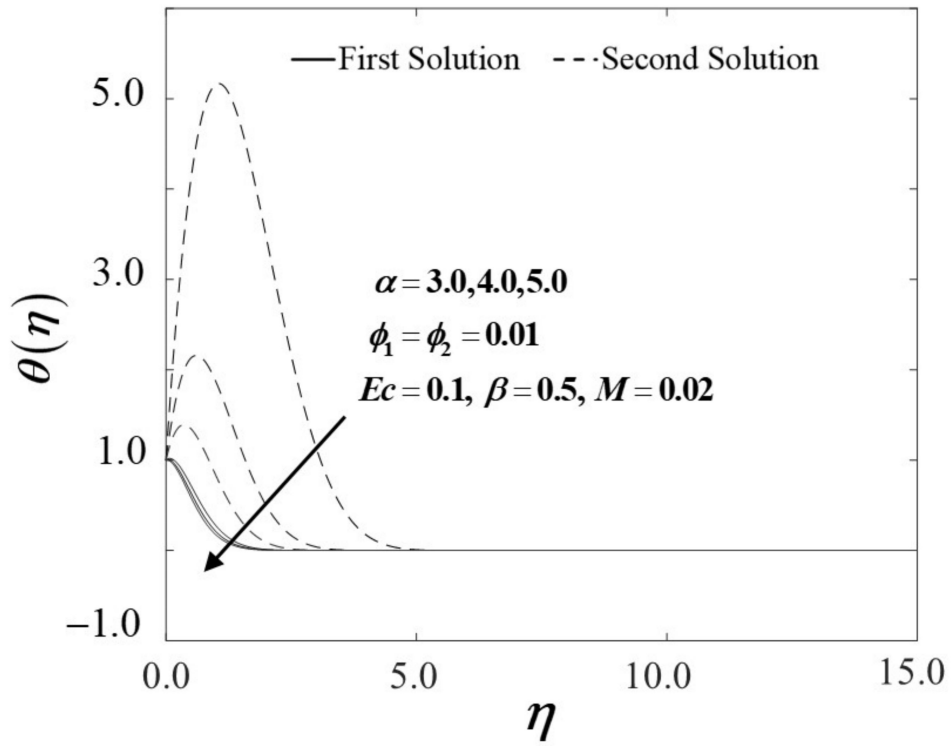

Figure 11. $\theta(\eta)$ versus η with specific α.

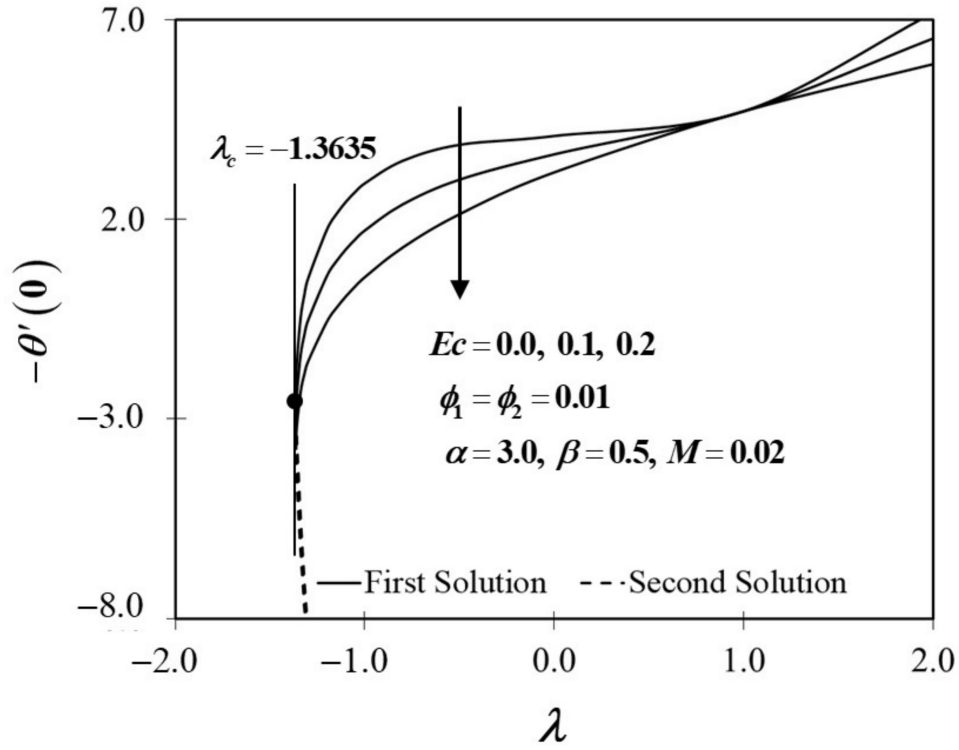

Figure 12. $-\theta'(0)$ versus λ with specific Ec.

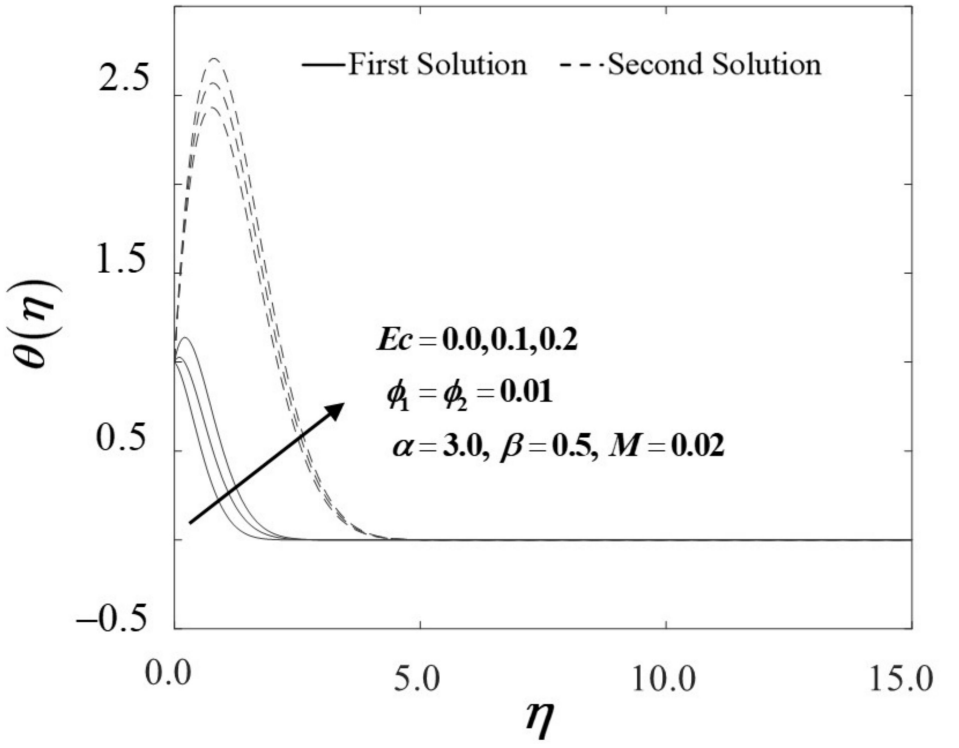

Figure 13. $\theta(\eta)$ versus η with specific Ec.

Table 3. Outcomes of $f''(0)$ with various λ when $\phi_1 = \phi_2 = \beta = M = Ec = 0$, $\alpha = 1.0$, and $\mathrm{Pr} = 6.2$.

λ	Current Result	Lok and Pop [45]	Ishak et al. [46]	Wang [47]
0.00	1.2325877	1.232590	1.232588	1.232588
0.10	1.1465610	1.146560	1.146561	1.146560
0.12	1.0511300	1.051130	1.051130	1.051130
0.50	0.7132950	0.713290	0.713295	0.713300
1.00	0.0000000	0.000000	0.000000	0.000000
2.00	−1.8873067	−1.887310	−1.887307	−1.887310
5.00	−10.2647493	−10.264750	−10.264749	−10.264750

The numerical values of $f''(0)$ and $-\theta'(0)$ as $\phi_1 = \phi_2 = 0.01$, $\alpha = 3.0$, $\beta = 0.5$, $Ec = 0.1$, and $\mathrm{Pr} = 6.2$ with various values of M are presented in Tables 4 and 5, respectively. According to Table 4, the values of skin friction on the shrinking sheet increase as the magnetic effects are enlarged. Based on the given values, the positive sign of $f''(0)$ indicates that a drag force is employed in the working fluid, while the negative sign of $f''(0)$ shows that the sheet exerts a dragging force on the flow field. Similarly, the values of heat transfer rate given by $|-\theta'(0)|$ demonstrate an increment trend as the magnetic effects are improved in hybrid nanofluid flow as accessible in Table 5. This appears to prove that the existence of a magnetic field in the flow environment may improve thermal efficiency.

Table 4. Values of $f''(0)$ as $\phi_1 = \phi_2 = 0.01$, $\alpha = 3.0$, $\beta = 0.5$, $Ec = 0.1$, and $\mathrm{Pr} = 6.2$.

λ	M = 0.00	M = 0.02	M = 0.09
−1.35	1.407433	1.518969	1.782108
−1.357	1.168339	1.400287	1.717588
−1.3571	1.152858	1.398211	1.716609
−1.36	-	1.328926	1.687407
−1.363	-	1.209601	1.655338
−1.3635	-	1.160063	1.649786
−1.37	-	-	1.570809
−1.38	-	-	1.405473
−1.3860	-	-	1.171852

Table 5. Values of $-\theta'(0)$ as $\phi_1 = \phi_2 = 0.01$, $\alpha = 3.0$, $\beta = 0.5$, $Ec = 0.1$, and $\mathrm{Pr} = 6.2$.

λ	M = 0.00	M = 0.02	M = 0.09
−1.35	−2.069568	−1.767616	−1.156300
−1.357	−2.924097	−2.150839	−1.343561
−1.3571	−2.985082	−2.157791	−1.346443
−1.36	-	−2.395452	−1.433040
−1.363	-	−2.833635	−1.529538
−1.3635	-	−3.028179	−1.546401
−1.37	-	-	−1.791562
−1.38	-	-	−2.342395
−1.3860	-	-	−3.239496

Moreover, it is noticed that there are two possible solutions in this study; therefore, an analysis of solution stability is necessary to obtain a consistent solution. The stability analysis technique reveals the properties of the dual solutions by identifying the smallest eigenvalue. As seen in Table 6, the first solution is reliable since ω_1 is positive, whereas the second solution is not since ω_1 is negative, which highlights the dissatisfying stabilising feature.

Table 6. The smallest eigenvalues ω_1 with assorted λ.

λ	First Solution	Second Solution
-1.2	0.8972	-0.9136
-1.3	0.8698	-0.8942
-1.33	0.3465	-0.4475
-1.363	0.1161	-0.2261
-1.3635	0.1020	-0.1382

In this study, the values of the governing parameters such as M, Ec, and λ are selected based on the availability of the dual solutions. Particularly, any values can be used in order to generate the results, as long as the profiles are asymptotically converged. However, the results may vary, and a unique solution is expected since a different range of the governing parameter is employed. On the other hand, the Pr value is fixed to 6.2 to indicate the base fluid state as water at 25°C. The reduced skin friction coefficients $f''(0)$ of viscous fluid $(\phi_1 = \phi_2 = 0.00)$, nanofluid $(\phi_1 = 0.00, \phi_2 = 0.01)$, and hybrid nanofluid $(\phi_1 = \phi_2 = 0.01)$ are available in Figure 2, while the heat transfer rate $-\theta'(0)$ is portrayed in Figure 3. It is observed that the similarity solutions for viscous flow $(\phi_1 = \phi_2 = 0.00)$ are available when $\lambda \geq \lambda_c = -1.3632$. The range of solution becomes wider when the nanoparticle volume fraction is added, where $\lambda \geq \lambda_c = -1.3633$ and $\lambda \geq \lambda_c = -1.3635$, which denote the Al_2O_3/H_2O nanofluid and Al_2O_3-Cu/H_2O hybrid nanofluid, respectively. However, for $\lambda \leq \lambda_c < 0$, the full partial differential Equations (1) to (3) should be numerically solved.

Figure 2 also indicates that the growth of ϕ particularly enhances the behaviour of $f''(0)$. Furthermore, in these three different types of fluids, the hybrid nanofluids show the highest trend of $f''(0)$ compared to conventional viscous fluid and nanofluid, particularly when 1% of ϕ_1 (Al_2O_3) and 1% of ϕ_2 (Cu) volume concentration are presented. Figure 3 depicts a positive expansion in $-\theta'(0)$, which represents the first solution's heat transfer rate. Overall, when the viscous flow transforms into Al_2O_3/H_2O and Al_2O_3-Cu/H_2O as it passes through the stretching/shrinking plate, the heat transfer capability improves.

The effect of a magnetic field M on this particular case is also worth exploring. The characteristics of skin friction coefficient $f''(0)$ and heat transfer rate $-\theta'(0)$ are presented in Figures 4 and 5, respectively. Based on the generated outcomes, the addition of M shows a response where both $f''(0)$ and $-\theta'(0)$ are increased when M improved. This is because of the Lorentz force, which is caused by the engagement of the induced electric currents and the applied magnetic field in the flow field. This accelerated flow increased the velocity gradient near the plate surface and intensified the velocity inside the boundary layer, escalating the trend of $f''(0)$ and $-\theta'(0)$. It is interesting to note that the presence of M when $M = 0.02, 0.09$ is proven to improve the efficiency of heat transfer performance compared to $M = 0.0$ since the first solution exhibits an upward trend, as displayed in Figure 5.

Figures 6 and 7 illustrate the unsteadiness parameter β influences towards the stretching/shrinking plate λ. The hybrid nanofluid Al_2O_3-Cu/H_2O characteristics are portrayed in Figure 6 concerning $f''(0)$ when $\beta > 0$. It is concluded that as β improved, the first solution has increased in $f''(0)$ while the response of the second solution was in the reverse direction. Additionally, $-\theta'(0)$ is currently improved when λ escalates in the first solution, as observed in Figure 7.

Figures 8–11 show the effect of the acceleration parameter α in regard to λ on the stretching/shrinking plate. Focusing on the first solution, Figure 8 illustrates that the increment of α spontaneously intensifies $f''(0)$. This finding also implies that a greater amount of α broadens the flow behaviour, causing the flow velocity to increase and decrease the boundary layer thickness, as displayed in Figure 10. In addition, Figure 8 also consequently observes the pattern of $f''(0) = 0$ as $\lambda = 1.0$. This is due to the no frictional drag force occurrences on the stretching sheet. Sequentially, Figure 9 depicts the thermal efficiency, with $-\theta'(0)$ intensifying in the first solution as the value of α increases in the hybrid nanofluid. The results demonstrate that increasing the acceleration parameter flow promotes thermal

conductivity effectively. The temperature profiles $\theta(\eta)$ in Figure 11 back up the trend seen in Figure 9, which shows the reduction in temperature distributions as α increases. The deterioration in Al_2O_3-Cu/H_2O temperature improves the thermal transmission and gradually upsurges the heat transfer performance. Based on Figures 10 and 11, it is noted that all profiles asymptotically satisfy the free stream conditions (8), which then authorises the validity of the numerical solutions.

Figures 12 and 13 demonstrate the impact of Ec on heat transfer rate $-\theta'(0)$ and temperature profile distributions $\theta(\eta)$. An increase in Ec contributes to the decrement of $-\theta'(0)$ in both solutions, as depicted in Figure 12. Furthermore, the development of Ec values does not delay the boundary layer separation of Al_2O_3-Cu/H_2O. In general, the Eckert number is the potential ratio of the advective transport and heat dissipation. Therefore, higher Eckert numbers generate more heat due to friction forces between fluid particles. This argument confirms the trend of $\theta(\eta)$ shown in Figure 13. Evidently, we can deduce that the Eckert number has a tendency to degrade heat conveyance performance in this particular case. To summarise, the generated results may be advantageous to various researchers, allowing the mathematical simulation outcomes to be as close to the actual situation as possible. In addition, the results discussed earlier may also provide better theoretical guidance for engineering applications and scientific research, especially in nanotechnology and thermal systems.

5. Conclusions

The current work verified the numerical assessment of the unsteady MHD boundary layer separated stagnation-point flow with viscous dissipation and Joule heating. A new mathematical hybrid nanofluid model was introduced, and the effects of various control factors were investigated. Since dual solutions are perceived in this study, a stability analysis is performed to confirm the reliability of the solutions. According to our findings, the presence of the first and second solutions is demonstrated for a wide range of control parameters throughout the dual-type nanoparticles, which consist of alumina (Al_2O_3) and copper (Cu). Apparently, Al_2O_3-Cu/H_2O shows higher thermal efficiency than pure water and nanofluid, which contains a single nanoparticle (Al_2O_3/H_2O). The addition of a nanoparticle volume fraction concentration can effectively boost the heat transfer rate in this study. Furthermore, the unsteadiness and acceleration parameter increments greatly stimulate the skin friction coefficient and thermal performance of Al_2O_3-Cu/H_2O. The inclusion of the Eckert number increased the temperature profile distribution and impulsively decreased the heat transfer rate. Consequently, the stability analysis ensures the consistency of the first solution. Future work of this study may consider other types of hybrid nanoparticles such as ZnO-TiO_2, Ag-CuO, or carbon nanotubes (CNTs). In addition, a different mathematical analysis approach, for example, Lie-group analysis or entropy generation analysis, can be employed as potential research.

Author Contributions: Methodology, N.A.Z. and I.P.; validation, N.A.Z., K.N. and R.N.; software, N.A.Z.; investigation, N.A.Z.; formal analysis, N.A.Z.; editing, K.N., R.N., I.P. and N.A.Z.; supervision, K.N., R.N. and I.P.; funding acquisition, R.N. All authors have read and agreed to the published version of the manuscript.

Funding: The Universiti Kebangsaan Malaysia has allocated GUP-2019-034 to this project.

Institutional Review Board Statement: Not applicable.

Informed Consent Statement: Not applicable.

Data Availability Statement: Not applicable.

Acknowledgments: The authors thank everyone who contributed to the establishment of this manuscript.

Conflicts of Interest: The authors declare no conflict of interest.

References

1. Huminic, G.; Huminic, A. Hybrid nanofluids for heat transfer applications—A state-of-the-art review. *Int. J. Heat Mass Transf.* **2018**, *125*, 82–103. [CrossRef]
2. Sidik, N.A.C.; Adamu, I.M.; Jamil, M.M.; Kefayati, G.H.R.; Mamat, R.; Najafi, G. Recent progress on hybrid nanofluids in heat transfer applications: A comprehensive review. *Int. Commun. Heat Mass Transf.* **2016**, *78*, 68–79. [CrossRef]
3. Suresh, S.; Venkitaraj, K.P.; Selvakumar, P. Synthesis, characterisation of Al_2O_3-Cu nano composite powder and water based nanofluids. *Adv. Mater. Res.* **2011**, *328–330*, 1560–1567. [CrossRef]
4. Rabiei, S.; Khosravi, R.; Bahiraei, M.; Raziei, M.; Hosseini, A.A. Thermal and hydraulic characteristics of a hybrid nanofluid containing graphene sheets decorated with platinum through a new wavy cylindrical microchannel. *Appl. Therm. Eng.* **2020**, *181*, 115981. [CrossRef]
5. Renuka, A.; Muthtamilselvan, M.; Al-Mdallal, Q.M.; Doh, D.H.; Abdalla, B. Unsteady separated stagnation point flow of nanofluid past a moving flat surface in the presence of Buongiorno's model. *J. Appl. Comput. Mech.* **2021**, *7*, 1283–1290.
6. Ur Rehman, A.; Abbas, Z. Stability analysis of heat transfer in nanomaterial flow of boundary layer towards a shrinking surface: Hybrid nanofluid versus nanofluid. *Alex. Eng. J.* **2022**, *61*, 10757–10768. [CrossRef]
7. Connolly, B.J.; Loth, E.; Smith, C.F. Unsteady separated flows in an S-Duct and a bifurcating duct. *J. Aircr.* **2022**, *59*, 47–57. [CrossRef]
8. Kamis, N.I.; Jiann, L.Y.; Shafie, S.; Khairuddin, T.K.A.; Md Basir, M.F. Magnetohydrodynamics boundary layer flow of hybrid nanofluid in a thin-film over an unsteady stretching permeable sheet. *J. Nanofluids* **2022**, *11*, 74–83. [CrossRef]
9. Nadeem, M.; Siddique, I.; Awrejcewicz, J.; Bilal, M. Numerical analysis of a second-grade fuzzy hybrid nanofluid flow and heat transfer over a permeable stretching/shrinking sheet. *Sci. Rep.* **2022**, *12*, 1631. [CrossRef]
10. Elsaid, E.M.; Abdel-wahed, M.S. Impact of hybrid nanofluid coolant on the boundary layer behavior over a moving cylinder: Numerical case study. *Case Stud. Therm. Eng.* **2021**, *25*, 100951. [CrossRef]
11. Hassan, M.; El-Zahar, E.R.; Khan, S.U.; Rahimi-Gorji, M.; Ahmad, A. Boundary layer flow pattern of heat and mass for homogenous shear thinning hybrid-nanofluid: An experimental data base modeling. *Numer. Methods Partial Differ. Equ.* **2021**, *37*, 1234–1249. [CrossRef]
12. Sheikholeslami, M. Numerical investigation of solar system equipped with innovative turbulator and hybrid nanofluid. *Sol. Energy Mater. Sol. Cells* **2022**, *243*, 111786. [CrossRef]
13. Khalili, N.N.W.; Samson, A.A.; Aziz, A.S.A.; Ali, Z.M. Chemical reaction and radiation effects on MHD flow past an exponentially stretching sheet with heat sink. *J. Phys. Conf. Ser.* **2017**, *890*, 12025. [CrossRef]
14. Devi, S.P.A.; Devi, S.S.U. Numerical investigation of hydromagnetic hybrid Cu–Al_2O_3/water nanofluid flow over a permeable stretching sheet with suction. *Int. J. Nonlinear Sci. Numer. Simul.* **2016**, *17*, 249–257. [CrossRef]
15. Zainal, N.A.; Nazar, R.; Naganthran, K.; Pop, I. MHD flow and heat transfer of hybrid nanofluid over a permeable moving surface in the presence of thermal radiation. *Int. J. Numer. Methods Heat Fluid Flow* **2021**, *31*, 858–879. [CrossRef]
16. Khashi'ie, N.S.; Waini, I.; Arifin, N.M.; Pop, I. Unsteady squeezing flow of Cu-Al_2O_3/water hybrid nanofluid in a horizontal channel with magnetic field. *Sci. Rep.* **2021**, *11*, 14128. [CrossRef]
17. Yashkun, U.; Zaimi, K.; Bakar, N.A.A.; Ishak, A.; Pop, I. MHD hybrid nanofluid flow over a permeable stretching/shrinking sheet with thermal radiation effect. *Int. J. Numer. Methods Heat Fluid Flow* **2021**, *31*, 1014–1031. [CrossRef]
18. Zainal, N.A.; Nazar, R.; Naganthran, K.; Pop, I. Stability analysis of MHD hybrid nanofluid flow over a stretching/shrinking sheet with quadratic velocity. *Alex. Eng. J.* **2021**, *60*, 915–926. [CrossRef]
19. Aly, E.H.; Abdelhalim, E. MHD Marangoni boundary layer problem for hybrid nanofluids with thermal radiation. *Int. J. Numer. Methods Heat Fluid Flow* **2021**, *31*, 897–913. [CrossRef]
20. Shafee, A.; Allahyari, M.; Ramzan, M.; Zaib, A.; Babazadeh, H. Modeling of MHD hybrid nanofluid flow through permeable enclosure. *Int. J. Mod. Phys. C* **2020**, *31*, 2050106. [CrossRef]
21. Dinarvand, S. Nodal/saddle stagnation-point boundary layer flow of CuO–Ag/water hybrid nanofluid: A novel hybridity model. *Microsyst. Technol.* **2019**, *25*, 2609–2623. [CrossRef]
22. Reddy, M.G.; Reddy, K.V. Influence of Joule heating on MHD peristaltic flow of a nanofluid with compliant walls. *Procedia Eng.* **2015**, *127*, 1002–1009. [CrossRef]
23. Sheikholeslami, M.; Ganji, D.D. Nanofluid hydrothermal behavior in existence of Lorentz forces considering Joule heating effect. *J. Mol. Liq.* **2016**, *224*, 526–537. [CrossRef]
24. Khashi'ie, N.S.; Arifin, N.M.; Pop, I.; Wahid, N.S. Flow and heat transfer of hybrid nanofluid over a permeable shrinking cylinder with Joule heating: A comparative analysis. *Alex. Eng. J.* **2020**, *59*, 1787–1798. [CrossRef]
25. Khashi'ie, N.S.; Arifin, N.M.; Pop, I. Magnetohydrodynamics (MHD) boundary layer flow of hybrid nanofluid over a moving plate with Joule heating. *Alex. Eng. J.* **2022**, *61*, 1938–1945. [CrossRef]
26. Naseem, T.; Urooj, F.; Mohammad, M.; Azeem, S.; Nasreen, K.; Kottakkaran, S.N.; Ahamed Saleel, C.; Mohamed, A. Joule heating and viscous dissipation effects in hydromagnetized boundary layer flow with variable temperature. *Case Stud. Therm. Eng.* **2022**, *35*, 102083. [CrossRef]
27. Daniel, Y.S.; Aziz, Z.A.; Ismail, Z.; Salah, F. Effects of thermal radiation, viscous and Joule heating on electrical MHD nanofluid with double stratification. *Chin. J. Phys.* **2017**, *55*, 630–651. [CrossRef]

28. Khan, M.I.; Qayyum, S.; Hayat, T.; Khan, M.I.; Alsaedi, A. Entropy optimisation in flow of Williamson nanofluid in the presence of chemical reaction and Joule heating. *Int. J. Heat Mass Transf.* **2019**, *133*, 959–967. [CrossRef]
29. Yan, L.; Dero, S.; Khan, I.; Mari, I.A.; Baleanu, D.; Nisar, K.S.; Sherif, E.S.M.; Abdo, H.S. Dual solutions and stability analysis of magnetised hybrid nanofluid with joule heating and multiple slip conditions. *Processes* **2020**, *8*, 332. [CrossRef]
30. Mahanthesh, B.; Gireesha, B.J.; Gorla, R.S.R. Unsteady three-dimensional MHD flow of a nano Eyring-Powell fluid past a convectively heated stretching sheet in the presence of thermal radiation, viscous dissipation and Joule heating. *J. Assoc. Arab Univ. Basic Appl. Sci.* **2017**, *23*, 75–84. [CrossRef]
31. Hayat, T.; Naseem, A.; Farooq, M.; Alsaedi, A. Unsteady MHD three-dimensional flow with viscous dissipation and Joule heating. *Eur. Phys. J. Plus* **2013**, *128*, 158. [CrossRef]
32. Chaudhary, S.; Choudhary, M.K. Viscous dissipation and Joule heating effects on an unsteady magnetohydrodynamic flow over a linearly stretching permeable surface with uniform wall temperature. *Indian J. Pure Appl. Phys.* **2017**, *55*, 864–872.
33. Ahmed, A.; Khan, M.; Ahmed, J.; Hafeez, A.; Iqbal, Z. Unsteady stagnation point flow of maxwell nanofluid over stretching disk with joule heating. *Arab. J. Sci. Eng.* **2020**, *45*, 5529–5540. [CrossRef]
34. Malekian, S.; Fathi, E.; Malekian, N.; Moghadasi, H.; Moghimi, M. Analytical and numerical investigations of unsteady graphene oxide nanofluid flow between two parallel plates. *Int. J. Thermophys.* **2018**, *39*, 100. [CrossRef]
35. Zainal, N.A.; Nazar, R.; Naganthran, K.; Pop, I. Unsteady flow of a Maxwell hybrid nanofluid past a stretching/shrinking surface with thermal radiation effect. *Appl. Math. Mech.* **2021**, *42*, 1511–1524. [CrossRef]
36. Zainal, N.A.; Nazar, R.; Naganthran, K.; Pop, I. Unsteady MHD stagnation point flow induced by exponentially permeable stretching/shrinking sheet of hybrid nanofluid. *Eng. Sci. Technol. Int. J.* **2021**, *24*, 1201–1210. [CrossRef]
37. Rehman, A.; Salleh, Z. Approximate analytical analysis of unsteady MHD mixed flow of non-Newtonian hybrid nanofluid over a stretching surface. *Fluids* **2021**, *6*, 138. [CrossRef]
38. Waini, I.; Khashi'ie, N.S.; Kasim, A.R.M.; Zainal, N.A.; Hamzah, K.B.; Arifin, N.M.; Pop, I. Unsteady Magnetohydrodynamics (MHD) Flow of Hybrid Ferrofluid Due to a Rotating Disk. *Mathematics* **2022**, *10*, 1658. [CrossRef]
39. Dholey, S. Magnetohydrodynamic unsteady separated stagnation-point flow of a viscous fluid over a moving plate. *Z. Angew. Math. Mech.* **2016**, *96*, 707–720. [CrossRef]
40. Takabi, B.; Salehi, S. Augmentation of the heat transfer performance of a sinusoidal corrugated enclosure by employing hybrid nanofluid. *Adv. Mech. Eng.* **2014**, *6*, 147059. [CrossRef]
41. Oztop, H.F.; Abu-Nada, E. Numerical study of natural convection in partially heated rectangular enclosures filled with nanofluids. *Int. J. Heat Fluid Flow* **2008**, *29*, 1326–1336. [CrossRef]
42. Merkin, J.H. On dual solutions occurring in mixed convection in a porous medium. *J. Eng. Math.* **1986**, *20*, 171–179. [CrossRef]
43. Weidman, P.D.; Kubitschek, D.G.; Davis, A.M.J. The effect of transpiration on self-similar boundary layer flow over moving surfaces. *Int. J. Eng. Sci.* **2006**, *44*, 730–737. [CrossRef]
44. Harris, S.D.; Ingham, D.B.; Pop, I. Mixed convection boundary-layer flow near the stagnation point on a vertical surface in a porous medium: Brinkman model with slip. *Transp. Porous Media* **2009**, *77*, 267–285. [CrossRef]
45. Lok, Y.Y.; Pop, I. Stretching or shrinking sheet problem for unsteady separated stagnation-point flow. *Meccanica* **2014**, *49*, 1479–1492. [CrossRef]
46. Ishak, A.; Lok, Y.Y.; Pop, I. Stagnation-point flow over a shrinking sheet in a micropolar fluid. *Chem. Eng. Commun.* **2010**, *197*, 1417–1427. [CrossRef]
47. Wang, C.Y. Stagnation flow towards a shrinking sheet. *Int. J. Non-Linear Mech.* **2008**, *43*, 377–382. [CrossRef]